GA–A24014

STABILIZATION OF THE RESISTIVE WALL MODE IN DIII–D BY PLASMA ROTATION AND MAGNETIC FEEDBACK

by

M. Okabayashi, J. Bialek, M.S. Chance, M.S. Chu,
E.D. Fredrickson, A.M. Garofalo, R. Hatcher, T.H. Jensen,
L.C. Johnson, R.J. La Haye, G.A. Navratil, H. Reimerdes,
J.T. Scoville, E.J. Strait, A.D. Turnbull, M.L. Walker,
and the DIII–D Team

SEPTEMBER 2002

DISCLAIMER

GA–A24014

STABILIZATION OF THE RESISTIVE WALL MODE IN DIII–D BY PLASMA ROTATION AND MAGNETIC FEEDBACK

by

M. Okabayashi,[1] J. Bialek,[2] M.S. Chance,[1] M.S. Chu,[3]
E.D. Fredrickson,[1] A.M. Garofalo,[2] R. Hatcher,[1] T.H. Jensen,[3]
L.C. Johnson,[1] R.J. La Haye,[2] G.A. Navratil,[2] H. Reimerdes,[2]
J.T. Scoville,[3] E.J. Strait,[3] A.D. Turnbull,[3] M.L. Walker,[3]
and the DIII–D Team

This is a preprint of a paper to be published in *Plasma Physics and Controlled Fusion.*

[1]Princeton Plasma Physics Laboratory, P.O. Box 451, Princeton, New Jersey 08544 USA
[2]Columbia University, New York, New York 10027 USA
[3]General Atomics, P.O. Box 85608, San Diego, California 92186-5608 USA

Work supported by
U.S. Department of Energy under
Contracts DE-AC02-76CH03073, DE-AC03-99ER54463,
and Grant DE-FG02-89ER53297

GENERAL ATOMICS PROJECT 30033
September 2002

ABSTRACT

Suppression of the resistive wall mode (RWM) has been successfully demonstrated in the DIII–D tokamak by using rotational stabilization in conjunction with a close-fitting vacuum vessel wall. The duration of the high-pressure discharge was extended to hundreds of the wall skin time. Frequently, the plasma pressure reached the ideal-wall MHD kink limit. The confined pressure is up to twice as high as the no-wall ideal MHD kink limit. Near its marginal stability point, the RWM is found to resonate with residual non-axisymmetric fields (e.g., components of the error field). A magnetic feedback system has been used to identify and compensate for the residual non-axi-symmetric fields. This is to the best of our knowledge, the first demonstration of the sustainment of a stable plasma with pressure at levels well above the no-wall pressure limit. This technique is expected to be applicable to other toroidal devices.

I. INTRODUCTION

Since the beginning of fusion plasma research, confinement concepts have been exploited aiming for long duration and stable high temperature plasmas. A minimum of plasma pressure is required to reach ignition and for economic reasons the magnetic pressure should be kept below the limit imposed by engineering considerations. Thus the value $\beta=p/(B_T^2/(2\pi\mu_o))$, here p is the plasma pressure and B_T is the toroidal field strength, has traditionally been regarded as a figure of merit for the fusion devices. The tokamak concept was originated as a pulsed operational device. It's potential of steady state operation is enhanced by the possibility of utilizing the "bootstrap current," which is generated by the plasma pressure. The utilization of the bootstrap current in maintaining the plasma current can be optimized by increasing the plasma pressure while keeping the total plasma current at a moderate level. The appropriate figure of merit of tokamak reactors with high bootstrap current fraction is therefore the normalized β, β_n. β_n is β in units of normalized current $I/(aB_T)$, namely $\beta_n = \beta/(I/aB_T)$, a is the plasma minor radius, and I is the plasma current. The advanced tokamak configuration utilizes currents with a high bootstrap current fraction while maintaining the plasma at a high value of β [1–3].

The macroscopic stability of the high pressure plasma is the prerequisite of any confinement devices. The magnetohydrodynamic (MHD) theory, which has proven to describe adequately the macro-stability behavior of the experimental plasmas, has predicted that a global external kink (EK) is a major obstacle for achieving high pressure plasmas attractive to commercial reactors. In particular, the performance of high bootstrap current configurations is considered to be limited by the EK.

The EK is a global MHD mode with the displacement extending to the plasma edge where it interacts with the outside vacuum vessel. The interaction gives rise to perturbed magnetic energy in the vacuum region which contributes to the stabilization of the EK. Thus, the EK can be stabilized passively if the plasma is surrounded by a perfectly conducting shell which is located

within some critical distance, r_{crit}. When the resistivity of the shell is taken into account, leakage of the perturbed magnetic flux through the resistive wall located within r_{crit} still makes RWM unstable. The free energy source of the RWM is the same as the EK, but its growth rate is reduced to τ_w, the time scale of flux diffusion through the resistive shell. Two methods have been proposed for the stabilization of the RWM. One is to enhance the perturbed magnetic energy outside of the plasma actively by using a feedback system which takes into account the characteristics of the RWM. The other is to dissipate the free energy inside the plasma through plasma rotation. Rotational stabilization by viscous dissipation was first proposed by Bondeson and Ward [4,5]. Several additional plasma dissipation mechanisms were subsequently proposed 6,7]. Results from recent theoretical MHD works have also stimulated experiments aimed at the suppression of the RWM [9–14].

The DIII–D device, a large tokamak, (major radius of 1.75 m, minor radius of 0.6 m, and 2/1 elongation) has been exploring various aspects of the RWM [15–24].

Recently, on DIII–D we have successfully demonstrated the suppression of the RWM, and sustained the plasma pressure well above the value given by $\beta_N^{no-wall}$. RWM suppression has been achieved by maintaining the plasma rotation assisted by the close-fitting vacuum vessel wall. The high pressure portion of the discharge was extended in excess of hundreds of wall skin times. Performance of rotation stabilization of the RWM strongly depends on the magnitude of resonant field amplification (RFA) [25]. It was found that the RWM resonates with residual non-axisymmetric fields (such as a component of the error field). The resonance with the non-axisymmetric field becomes stronger as the discharge approaches the condition of marginal MHD stability. An increase in the mode amplitude of the RWM by this resonance enhanced the drag due to the electromagnetic torque induced in the plasma and decreased the plasma rotation velocity. The RFA can be minimized by reducing the residual resonant field. When the RFA is detected by a sensor, the magnetic feedback system is energized to reduce the RFA effect and simultaneously to reduce the residual un-compensated resonant non-axisymmetric field. Thus, the feedback actuator (i.e., the coil system) performs the double duties of error field correction as

well as mode suppression through the feedback process. Both of these functions of the feedback system are supported by direct experimental evidences.

II. STABILITY OF THE RESISTIVE WALL MODE

A. The basic dispersion relation for the EK and RWM

A qualitative understanding of the RWM physics, including its stabilization by plasma rotation and dissipation, can be obtained by examining a useful dispersion relation describing the energy balance as proposed by Chu [26]

$$(\gamma\tau_w + i\Omega_\phi\tau_w)^2(\kappa/\tau_w^2) + (\gamma\tau_w + i\Omega_\phi\tau_w)(\alpha/\tau_w) + \delta W_p + (\delta W_v^b\gamma\tau_w + \delta W_v^\infty)/(\gamma\tau_w + 1) = 0 \quad , \tag{1}$$

where τ_w is the skin penetration time of the vacuum vessel wall, Ω_ϕ is the angular rotational frequency, δW_p is the plasma potential energy, δW_v^b is the vacuum energy stored to the wall, δW_v^∞ is the vacuum energy stored to the infinity, and κ and α represent the strengths of the kinetic energy and plasma dissipation terms relative to the plasma potential energy respectively. The stability of the EK in a non-rotating plasma and without taking into account the resistivity of the wall ($\tau_w = 0$) is described by Eq. (1) by taking $\Omega_\phi = 0$. With no external wall ($\tau_w = 0$), the plasma is unstable if $\beta_n > \beta_n^{no-wall}$. Whereas for an ideal wall ($\tau_w = \infty$), the plasma is stable up to the $\beta_n^{no-wall}$ limit [Fig. 1(a)]. The growth rate of the EK is large and usually of the order of Alfvén frequency. When the finite conductivity of resistive wall is taken into account, a new branch, the RWM branch appears in the range of β_n ($\beta_n^{no-wall} < \beta_n < \beta_n^{no-wall}$) that was stabilized by an ideal conducting wall. However, although the RWM is unstable, the growth rate is only the order of τ_w, the resistive skin time of the wall, and is much slower than the characteristic Alfvén frequency of EK [Fig. 1(b)].

The magnetic feedback stabilization approach takes advantage of the greatly reduced growth rate of the RWM. This was proposed by [9,10]. For slowly growing modes, it can be feedback stabilized by a system with a modest power supply, since the feedback merely has to replace the flux loss through the vacuum vessel which is taking place over the skin time τ_w. With a low

feedback gain, a stable domain starts to appear at the $\beta_n^{no-wall}$ limit. The stable area is extended to higher β_n by increasing the feedback gain [Fig. 1(b)]. With plasma rotation and dissipation, first without considering feedback, the stability of the RWM is modified by their combined effect, $\alpha\Omega_\phi$ in Eq. (1). At a critical plasma rotation frequency, a stability window first appears if the β_n value is close to the $\beta_n^{no-wall}$. The size of the stability window increases with plasma rotation and dissipation. This dependence is shown in Fig. 1(c). It is interesting to note that increasing $\alpha\Omega_\phi$, extends the stability window towards lower value of β_n. Above a critical value of $\alpha\Omega_\phi$, complete stable path from low to the β_n to the ideal limit $\beta_n^{no-wall}$ appears.

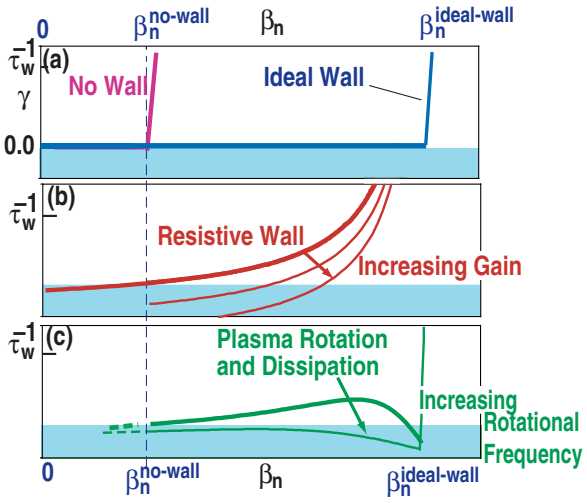

Fig. 1. Growth rates of the external kink mode as a function of the normalized plasma pressure (β_n). Shown are (a) stabilization of the external kink mode by an ideal wall, (b) stability of the RWM branch of the external kink mode for an ideal wall with a finite conductivity and the stabilization of the RWM by magnetic feedback by increased amount of feedback gain, (c) stabilization of the RWM by increased amount of plasma rotation and dissipation.

B. Resonant Field Amplification (RFA)

Boozer [25] proposed that near marginal stability, the plasma has a resonant response to the component of the non-axisymmetric external field (i.e., the error field) which has the mode structure of the RWM. Through this process, the plasma responses to other components of the error field are filtered. The spatial structure, helicity (the toroidal/poloidal (m/n) harmonic content of the response are therefore dominated by that of the RWM. The amplitude of the

response is also proportion to the resonant component in the external field. For a rotating plasma with dissipation effect, the plasma response is characterized by a finite toroidal phase shift relative to the input, caused by the rotational drag.

To compare the ansatz of Boozer's theory with experimental observations, in this section we introduce the extended lumped parameter model [27,28], which was used previously in the study of the feedback stabilization of the RWM.

One of the important elements of the lumped parameter model is the representation of the plasma response as a current with an effective inductance L_{eff}. The L_{eff} is obtained by noting that the energy and momentum flux balance across the plasma boundary is given by

$$a(d\xi/dr)/\xi|_a - 2/f + \alpha(\gamma + in\Omega_\phi) + \kappa(\gamma+in\Omega_\phi)^2 = a(d\psi/dr)/\psi|_a \quad . \qquad (2)$$

Here, ξ and ψ are the plasma displacement and the perturbed flux at the plasma boundary. The dissipation effect represented by α, and the kinetic energy contribution represented by κ are the generalizations to Ref. [27,28]. They can be identified with the corresponding terms in the δW formulation of Eq. (1). For a cylindrical plasma, f = m-nq. The no-wall stability point is given by f=1. It does not depend explicitly on the value of plasma β or β_n. For a toroidal plasma, the actual value of the equivalent parameter depends on the plasma pressure p and safety factor q profile. It can only be obtained by a complete solution of the plasma displacement within the plasma. For the present purpose, we choose f to retain its property of f=1 at no-wall stability for the β_n driven EK ($\beta_n/\beta_n^{no-wall} = 1$). This may be achieved by relating f to β_n through $\beta_n/\beta_n^{no-wall} = 2/f - 1$. We also adjust the wall location so that $\beta_n/\beta_n^{no-wall} = 2$ corresponds to ideal-wall limit. Although this adjustment introduces the plasma pressure in an adhoc manner, this introduction of the pressure into the cylindrical model has been found to be adequate in a previous study of the RWM growth rate [29,30].

In equivalent circuit with slow time limit (such as a quasi-steady-state operation), the perturbed flux ψ at the plasma surface has contributions due to each of the current components $\psi=\Sigma_j C_{ij}\delta I_j$. Conservation of the flux at a is expressed by

$$L_{eff}\delta I_p + C_{wp}\delta I_w + C_{cp}\delta I_c = 0 \quad , \qquad (3)$$

where,

$$L_{eff} = (\beta_o - 2/f + 1 + \kappa\,\Omega_\phi^2 + i\,\alpha\,\Omega_\phi)/(\beta_o - 2/f - 1 + \kappa\,\Omega_\phi^2 + i\,\alpha\,\Omega_\phi) \quad . \tag{4}$$

The subscripts (p, w, c,) correspond to quantities at the plasma, the resistive wall, and the external (active or error field) coil respectively. The C_{ij}s are the mutual inductances between the circuits δI_p, δI_w, and δI_c, corresponding to the plasma skin current representing the helical distortion, the passive wall eddy current, and the external coil current respectively. Since Eq. (2) multiplied by ψa^2 corresponds to the energy (flux) across the plasma surface, and magnetic flux is proportional to currents, the expression in Eq. (2) can be identified as an effective inductance L_{eff}. In Eq. (4), $\beta_0 = a(d\xi/dr)/\xi|_a$ is to be determined from an eigenvalue calculation, once the equilibrium profile is given. For a flat current profile, $\beta_0 = 1$. Experimentally, the parameter, β_0, can be determined through the marginal condition as discussed later.

When the eddy current in the resistive wall is negligible, which correspond to the situation of a quasi-steady evolution of the plasma in the presence of an external helical field, Eq. (4) may be solved to give

$$\delta I_p = (-C_{cp}/L_{eff})\,\delta I_c \quad . \tag{5}$$

This is the content of RFA. In Eq. (5), we have shown explicitly that the amplification and the toroidal phase shift in RFA are governed by the two parameters L_{eff} and Ccp (the mutual inductance between the plasma mode and external coils). Both of these can be obtained once the mode structure is determined.

Without the external error field and with the inclusion of the resistive wall current, the growth (or damping) rate of the RWM is given by [27,28]

$$\gamma\tau_w = L_{eff}/(L_{eff} - C^2_{cw}/L_{eff}) \quad . \tag{6}$$

This is also the expected damping rate after the RWM is deliberately excited by the application of an external resonant perturbation and then subsequently removed as used in the present experiment (Section 3).

A typical parametric dependence of the amplitude, the toroidal phase shift, and the damping rate on β_n resulting from RFA is shown in Fig. 2. A unique feature of RFA is that the amplitude

reaches a maximum when the stability condition is at marginal. The marginal stability condition, $\mathrm{Re}(\gamma\tau_w) = 0$, corresponds to $\mathrm{Re}\,(L_{eff}) \approx 0$ [Eq. (6)] so that the value of $\beta_n/\beta_n^{no-wall}$ at the marginal condition, β_{nc}, gives the value β_0 (assuming that the kinetic effect is negligible)

$$\beta_0 \approx \beta_{nc}/\beta_n^{no-wall} \quad . \tag{7}$$

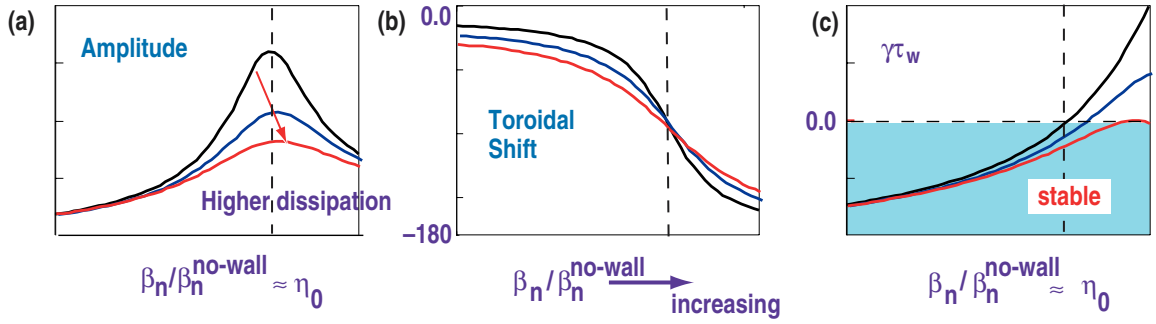

Fig. 2. Parametric dependence of various quantities on $\beta_n/(I/\pi a^-)$ RFA (resonant field amplification) predicted by the cylindrical lumped circuit model. The (black, blue, red) curves are for (low, medium , high) plasma dissipations. Shown are the dependence of (a) the amplitude of plasma response, (b) toroidal phase shift of plasma response relative to the input resonant field and (c) intrinsic growth (damping) rate of the plasma response.

In the rotating plasma, as in the induction motor, a phase shift between the applied external field from δI_c and the reacting field δB_p gives rise to an electromagnetic torque which decelerates the plasma rotation. The resultant torque can be related through Eq. (5) to be

$$\begin{aligned} d\Omega\phi/dt &= m_{in}/R^2 - (1/\rho_i R)\left(I/\pi a^2\right)\mathrm{Im}\left(\delta B_p \delta I_c\right) \\ &= m_{in}/R^2 - (1/\rho_i R)\left(I/\pi a^2\right)\left(C_{pc}/\alpha\Omega_\phi\right)(\delta I_c)^2 \end{aligned} \quad , \tag{8}$$

where m_{in} is the angular momentum density input per unit mass density and ρ_i is the ion mass density. In the application of Eq. (5), we have given the estimate for L_{eff} assuming that the plasma is near marginal stability ($\beta_{nc}/\left(I/\pi a^2\right) \approx \beta_0$). The deceleration term itself depends on the rotation as $(1/\alpha\Omega\phi)$. Once the rotation started decreasing, the reduction of the rotation velocity accelerates in time if the input of angular momentum input is too small. The dynamic relationship between the rotation and mode amplitude was discussed in detail in Ref. [17].

III. EXPERIMENTAL OBSERVATIONS OF RFA AND RWM

A. Observation of RFA

Shown in Fig. 3 are the schematic diagrams of the locations of the active feedback coils and magnetic field sensors on the DIII–D device. Shown in Fig. 3(a) are the six window frame feedback coils, called C-coils. They are shown in red and located on the midplane outside of the vacuum vessel. These coils produce non-axi-symmetric magnetic fields. Different combinations of currents in these coils can produce magnetic fields to: (1) compensate the residual error field, (2) supply a prescribed non-axi-symmetric field to the plasma, and (3) perform the function of the active feedback. Coils located 180° apart are connected in anti-series. Each pair is energized by an independent power supply, so that perturbed magnetic fields with both n=1 and 3 toroidal mode numbers can be produced. It should be noted that the applied active field, being produced by a single set of window frame coils located on the outboard midplane, does not have a preferred left- or right-handed helicity.

Shown in Fig. 3(b) are the various magnetic sensors installed both inside and outside the vessel. To maximize the n=1 component and to reject the even components, magnetic signals from pairs of sensors installed at toroidally diametric locations are combined before input to the feedback system. These sensors include the 3 pairs of external δBr saddle loops, the 6 pairs of internal δBr saddle loops, and the 4 pairs of the internal δBp probes. Several control schemes are possible using these sensors. The “smart shell” logic attempts to minimize the total flux (from both the plasma and the feedback coils) by compensating the leakage of the helical flux through the resistive wall to simulate a virtual ideal shell [9,10]. The smart shell approach uses the perturbed δB_r flux through the δB_r saddle loops, which detect the total radial flux penetrated through the resistive shell surface. Another scheme is the “mode control” approach which uses the signal originating solely from the plasma surface displacement without including signal from

the active coil currents. The mode control scheme has been found to work best by utilizing poloidal δB_p probes located inside the vacuum vessel [17,18]. It was also carried out to obtain feedback signals sensitive dominantly to the mode itself using external δB_r saddle loops signals compensated by C-coil currents ("explicit mode control") [19].

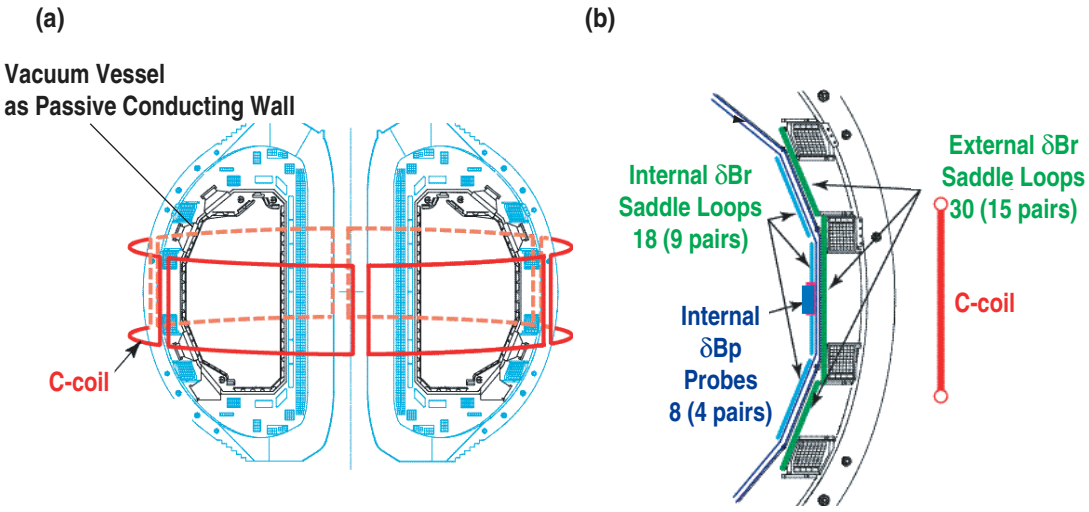

Fig. 3. Hardware arrangements. Shown in (a) in red are the 3 pairs of C-coils (feedback coils) which are energized by 3 independent power supplies. Different combination of currents in these coils serve to produce external magnetic fields that correct the error field, produce prescribed amount of extra non-axi-symmetric fields, and supply the active feedback magnetic field. Shown in (b) are three types of sensors: the external δB_r saddle loops (radial sensors), which sense perturbed radial field outside the vacuum wall, the internal δB_r saddle loops inside the vacuum wall, and the internal δB_p probes (poloidal field sensors) inside the vacuum vessel.

The importance of RFA to the RWM is shown in Fig. 4. In this figure, we show an attempt at exploring the effectiveness of plasma rotation in stabilizing the RWM as shown in Fig. 1(c) without first making corrections for RFA. Shown in red is the time history of a reference discharge. Shown in green is the time history of the discharge with its rotation increased by 50%–80% through increased angular momentum input with NBI at constant input power. It is seen that increasing the rotation alone without minimizing the resonant error field results in the excitation of a small amplitude RWM ($\approx$ 1 G) as the pressure increases above the no-wall stability limit. The RWM slows down the plasma rotation. Once the plasma rotation velocity decreased below a critical value, the discharge continued to a final β collapse. This observation suggests that RFA is occurring above $\left(I/\pi a^2\right)$ so that some residual non-axisymmetric field at a

non-negligible level resonates with the stable RWM. The amplified stable RWM reduces the plasma rotation velocity through the electromagnetic torque as discussed by Eq. (8) and leads to loss of the rotational stabilization and the β collapse.

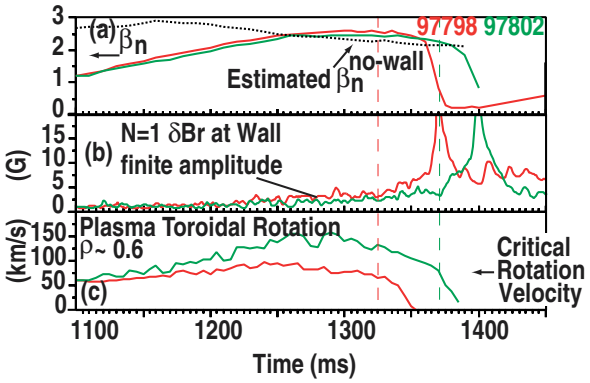

Fig. 4. Demonstration of rotational stabilization of the RWM by using increasing amount of angular momentum input. The trace in green (shot 97802) has a higher input of neutral beam angular momentum than the trace in red (shot 97798). Shown in different panels are (a) β_n, (b) amplitude of n=1 RWM , and (c) plasma toroidal rotation velocity at ρ~0.6 as a function of time. It is seen that with higher momentum input, both the plasma βn and rotation can be sustained for a longer time, and the onset of the resistive wall mode is delayed. It is also noted that the onset of the growth of the RWM appears to coincide with the reduction of the toroidal rotation velocity below a critical value.

B. Spatial resonant nature of the RFA process

To clearly demonstrate the existence of the RFA process, experiments were performed by deliberately applying an external non-axi-symmetric field produced by the C-coils. Figure 5 shows the response flux of the plasma during this RFA demonstration measured by the external δB_r saddle loops for three different discharges. Fig. 5(a) shows in (red, blue, and green) the development of β_n in time for a discharge (above, at, below) the no-wall β limit. Fig. 5(b) shows the time dependence of the applied perturbation field at the 2/1 surface. Fig. 5(c) shows the measured n=1 δB_r field due to the plasma at the resistive wall. Here, the direct signal at the wall from the C-coil currents has been subtracted. We see that the response from the plasma is larger when the plasma β is above the no-wall limit. Furthermore, the plasma responses all decay after the termination of the external pulse. This indicates that the RWM's are excited by the RFA

process to a finite amplitude. The plasma configuration is stable to the n = 1 external kink, even for the discharge shown in red. It is stabilized by plasma rotation even though its β_n is well above the no-wall limit.

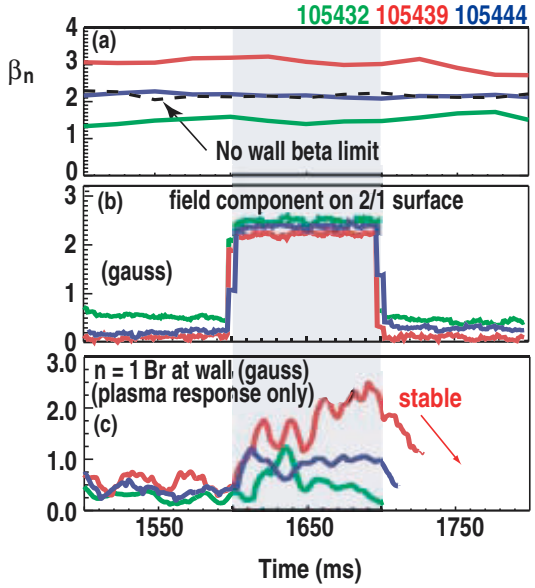

Fig. 5. Experimental observation of the Resonant Field Amplification (RFA) by applying a pulsed n=1 field. Shown are the time dependent variations of (a) β_n, (b) field amplitude of the n=1 external magnetic field on the 2/1 surface (The vacuum 2/1 field component was estimated using the actual geometry of the C-coil), and (c) the plasma response (of RFA) at the wall observed by the radial sensors located outside the vessel. The plasma response was obtained by subtracting the measured magnetic field with the same C-coil currents yet without the plasma present from that with the plasma. The curves in (red, blue, green) are for plasma β_n (above, at, below) the no wall β limit.

Figure 6 shows the spatial dependence of the plasma response to a pulsed n = 1 field. The plasma response was measured by the upper, midplane, and lower internal δB_r saddle loop arrays located inside the vacuum vessel. As mentioned previously, the C-coil system located at the outboard midplane does not produce perturbed magnetic field with a preferred helicity content. Without plasma, the toroidal phases observed on the upper, midplane and lower arrays were identical to that of the applied field. With plasma, a toroidal phase shift ≈ 20° in the direction of plasma rotation was observed between the phase of the midplane internal δB_r saddle loop signal and that of the input from C-coil, indicating that the mode structure was dragged along by the viscosity of the plasma. The upper and lower arrays show that the toroidal phases of the plasma

response are shifted to either higher or lower toroidal angles, in accordance with that expected from a helical mode structure. The upper/lower phase shifts are consistent with an m = +3 mode, which is also consistent with that expected from an external kink mode with the detector placed at the locations of the sensors. These observations of the toroidal phase shift as well as the mode pattern support the RFA concept given in Section 2.2.

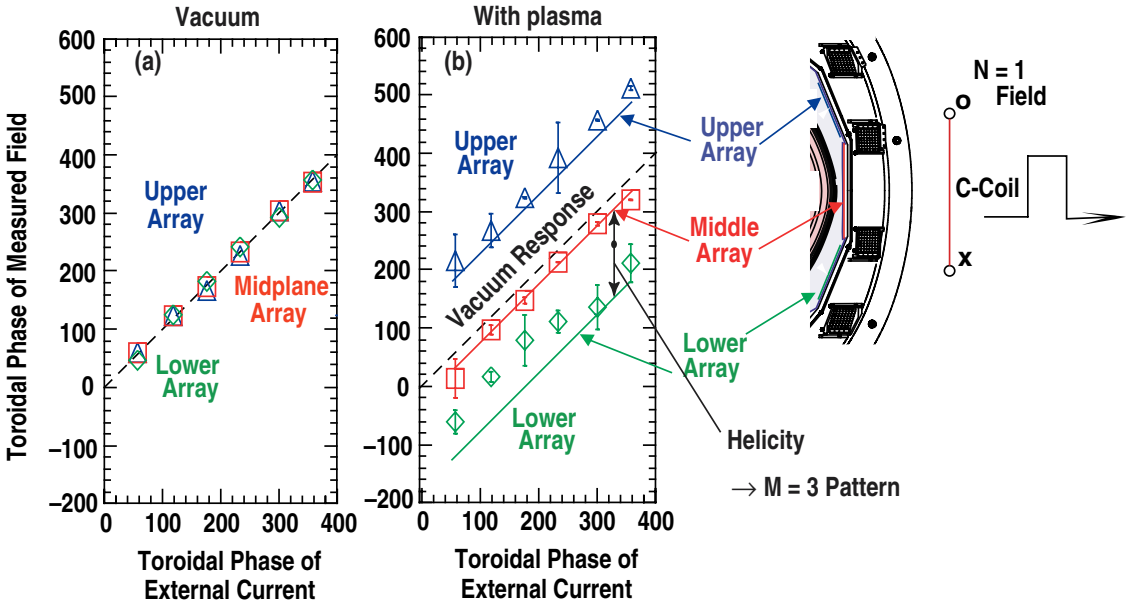

Fig. 6. The toroidal phase of the measured n=1 radial magnetic field (by the internal saddle loop array) as a function of the toroidal phase of the external current (a) without, and (b) with the plasma present poloidal structure with n=1 pulsed filed. Without plasma the phases of the upper, midplane, and lower probes coincide; with the plasma present, the measurements of the upper array show a constant advance in phase relative to those at the midplane, whereas the lower array show a similar amount of phase retardation; indicating a "resonant" response from the plasma.

The deceleration of plasma rotation by the electromagnetic torque discussed in Section 2.2 was studied by varying the magnitude of the external n = 1 field perturbation. Shown in Fig. 7(a) is the dependence of the plasma rotation frequency at the q = 2 surface on the magnitude of the external field. With a larger applied n = 1 field, the plasma slows down at a faster rate. In Fig. 7(b), the deceleration rate is plotted against the amplitude of the applied field squared divided by the rotational velocity, $(B_{ext}^2/(\Omega_\phi/2\pi)$, the characteristic parameter for the electromagnetic torque deceleration shown in Eq. (8). The observed linear dependence suggests that the RWM dynamics is in the high viscosity regime. In principle, it would be possible to

compare the observed deceleration rate with the estimates by the application of Eq. (8). However, there is too large an uncertainty in the geometrical factor in Eq. (8) to warrant such a comparison. The detailed parametric study with the inclusion of a more appropriate geometric factor is left another analysis [21,23].

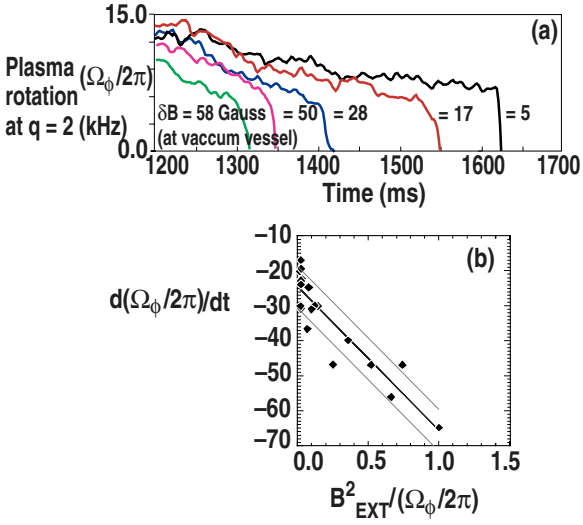

Fig. 7. Effect of the electromagnetic torque on plasma rotation. Shown are (a) the measured rotation frequency of the plasma at the q=2 surface as a function of time for different magnitudes (58, 50, 28, 17, 5 G) of the perturbed n =1 radial field (δB_r) measured at the vacuum vessel. (b) The deceleration rate vs. the torque parameter $B_{ext}^2/(\Omega_\phi/2\pi)$. In B_{ext} both the applied resonant field and the estimated residual error field are included [18,19].

C. Mode amplitude, phase and damping rate of RFA

An extensive study of the dependence of RFA on the normalized plasma beta β_n was carried out by applying the pulsed n = 1 fields. The magnitude of n=1 pluse field was kept small enough not to perturb the plasma rotation. The plasma rotation was maintained well above the critical velocity to minimize the impact by the electromagnetic torque by the applied field. A few examples of the plasma response and the damping behavior at the end of the pulse are shown in Fig. 5. Shown in Fig. 8(a) is the dependence of the mode amplitude, which is proportional to the amplification factor, on β_n. The amplification factor is observed to increase with β_n. The toroidal phase shift is shown in Fig. 8(b). The phase shift is in the direction of plasma rotation (opposite

to that of neutral beam injection) and increases with increasing β_n. Figure 8(c) shows the dependence of the RFA damping rate $|\gamma\tau_w|$ on β_n. The damping rate is the largest at $\beta_n/\left(I/\pi a^2\right)$ ≈1 and approaches the marginal condition, $|\gamma\tau_w|$ ≈ zero around $\beta_n/\left(I/\pi a^2\right)$ = 1.3–1.5. According to Eq. (7), the value of $\beta_n/\left(I/\pi a^2\right)$ at the marginal stability condition determines the profile parameter β_0. These dependencies are consistent with the discussion given in Section 2.2.

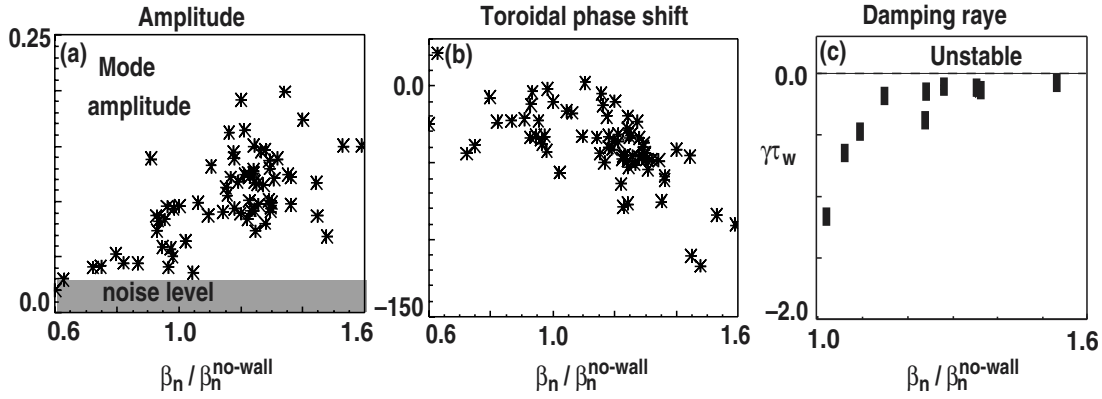

Fig. 8. The dependence of the various quantities in the RFA experiment on $\beta_n/\left(I/\pi a\right)$. The time dependence of the magnetic pulse used in the experiment was shown in Fig.5(b). Shown in the various panels are (a) the observed amplification factor versus β_n, (b) the observed toroidal phase shift versus β_n, and (c) the observed growth(damping) rate versus β_n. These figures should be compared with the corresponding figures shown in Fig. 2 obtained from the cylindrical lumped parameter model.

Following the discussion in Section 2.2 and neglecting the kinetic energy in the strong dissipation regime, we may proceed to understand the characteristics of the plasma dissipation during the RFA process. First, based on the behavior of the damping rate $|\gamma\tau_w|$ at the marginal stability point shown in Fig. (8c), the profile parameter β_0 is set to 1.3–1.5. The remaining unknown α was determined by minimizing the scatter of the observed amplitude and the toroidal phase shift relative to the predictions given by Eq. (5). Figure 9(a) shows the residue of the fit versus the value of α chosen with different values of β_0. It is seen that the residue shows the deepest minimum at β_0 = 1.5 and α =2.5 μs. The parameter α = 2.5 μs could be compared with the Alfvén transit time τ_A to obtain a measure of the effect of dissipation as α/τ_A ≈ 6–10. With this value of α, the ratio of the dissipation to the damping rate, $\alpha\Omega\phi/|\gamma\tau_w|$ can be obtained both experimentally and according to the cylindrical lumped circuit model. Shown in Fig. (8b) is

dependence of $\alpha\Omega\phi/|\gamma\tau_w|$ as a function of β_n both according to the cylindrical model and that from the experiment. It is seen that this ratio obtained both from direct experimental observation and also inferred from the model is in the range of 0.5–2, indicating that the dissipation effect dominates over the kinetic energy term. Fixing the value of $\alpha = 2.5$ μs with $\beta_0 = 1.5$ completes the cylindrical lumped circuit model. Figure 9(c,d,e) shows the comparison of the (amplitude, poloidal phase shift, damping rate) obtained from the cylindrical model with the corresponding quantities observed in the experiment. We observe that there is reasonable agreement for all three quantities.

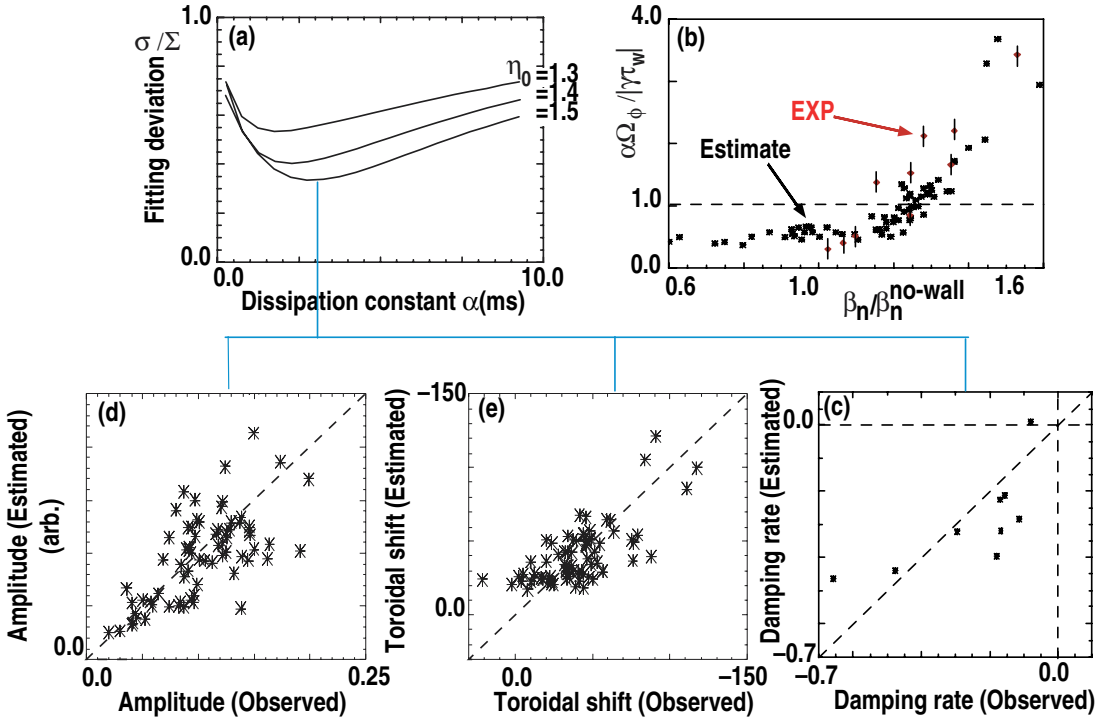

Fig. 9. Determination of the dissipation parameter α from results of the RFA experiments. Shown in (a) is the residue of the fit as a function of α for different values of β_0. It is seen that the value of $\beta_0 = 1.5$ gives the deepest minimum in the residue. Shown in (b) is the ratio of the effect of dissipation $|\alpha\Omega_\phi|$ to the damping rate $|\gamma\tau_w|$. The points with error bars are taken from experimental measurements. Points marked with * are estimates by applying the results from the cylindrical lumped circuit model. It is seen that this curve shows a break around $\beta_n/\beta_{nowall} = 1.0$. The unknown parameters in the cylindrical model are thus fixed with $\beta_0 = 1.5$ and $\alpha = 2.5$ μs. Shown in (c,d,e) are the estimated (damping rates, amplitudes, toroidal phase shifts) from the model plotted against those from observation.

We note that for this series of experiments, the critical β_n for the RFA onset does not seem to be near $\left(I/\pi a^2\right)$. This is a major difference from the original discussion of RFA advanced by

Boozer. However, we point out that there are other phenomenon not fully understood, such as the strong beta collapse near the $\left(I/\pi a^2\right)$ limit shown in Fig. 4. It is possible that the critical β_n depends on the other factors such as plasma rotation velocity. The parametric dependence of the critical β_n on these factors remains to be studied. It should also be noted that some other details are not well explained within the simple model. For example, the present model cannot explain the more drastic reduction of plasma response below the $\left(I/\pi a^2\right)$ limit observed in the experiment; while the cylindrical model shows a more gradual change of this response when plasma β_n is increased across the $\left(I/\pi a^2\right)$ limit.

IV. ACCESSING THE HIGH β_n REGIME

As shown in the example of rotational stabilization (Fig. 5), RFA takes place at $\beta_n \geq \left(I/\pi a^2\right)$. The perturbed field from RFA starts small at the onset and becomes more prominent and easily detectable later in time. Therefore, the "growth" of RFA should be preventable by using magnetic feedback and a highly sensitive sensor for its early detection. In this scenario, the magnetic sensors detect the perturbed magnetic field resulting from the RFA amplification and the feedback coils are activated to minimize the sensor signal. Thus the feedback is utilized to find the residual non-axisymmetric component and to minimize it. This indicates another alternative that once the non-axisymmetric component is found, the field compensation could also be achieved by pre-programming the C-coils for the discharge without relying on the feedback action to the signals from the sensors. The schematic flow diagrams for these two alternative routes for the feedback loops are shown in Fig. 10(a). Shown in Fig. 10(b) is the schematic of the effect of increasing rotation and increasing feedback gain on the stabilization of the RWM. Experimentally, it was found that the poloidal sensor is the best in sensing the onset of RFA, as the poloidal sensor does not couple directly to the active feedback coils [21]. It was also possible to provide feedback signals sensitive dominantly to the plasma mode using external δB_r saddle loop signals and coil current "Explicit Mode Control". In this approach the signal observed by the external flux loop needs the compensation of flux due to the direct coupling to the active coil. As reported in Ref. [19], it was successful to produce the long duration discharges when the compensation of flux due to the vacuum vessel eddy current was included.

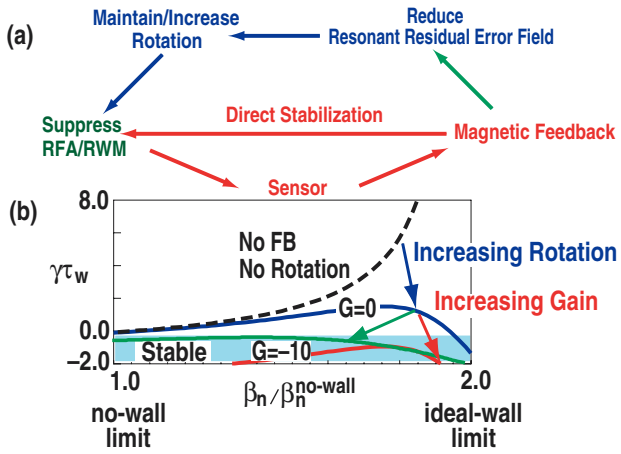

Fig. 10. Schematic of the flow diagram and the integration of the feedback system (a) The schematic diagram of the magnetic feedback stabilization. This diagram shows that the RWM/RFA can be stabilized either through the loop of sensor(magnetic feedback)–direct stabilization or through the line of magnetic feedback-(reducing resonant error field)-maintain/increase rotation. Shown in (b) is the dependence of the growth rate on these two routes for RWM stabilization. Either increasing rotation or increasing the feedback gain can push the curve of growth rate below the $\gamma\tau_w$=0 line.

A. Achieving the ideal kink limit

Figure 11 shows the achievement of high β_n close to the β limit by utilizing activation of the magnetic feedback. The achieved β_n was twice the no-wall β limit which is close to the ideal-wall kink limit. This is, to the best of our knowledge, the first achievement of the ideal-wall pressure limit at such a high level of $\beta_n/\left(I/\pi a^2\right)$. The discharge utilized a modest current ramp entered the lower q-edge operation regime. The discharge termination occurred with $q_{95} \approx 3.1$ and was accompanied by a fast growing n =1 precursor. The observed 300 μs growth time for the precursor is explainable as the onset of an ideal kink taking into account the evolution in time of the equilibrium [31,32]. The ideal MHD stability computation with a series of numerical equilibria reconstructed from experimental data indicates that the experimental configuration is within 10% of the ideal-wall β limit. In the feedback process, the demand signal to the feedback system was a signal with a gradual change to the coil currents, indicating that the signals detected by the poloidal sensors are from RFA excited by some residual resonant component of the non-axisymmetric (error) field which evolves in time.

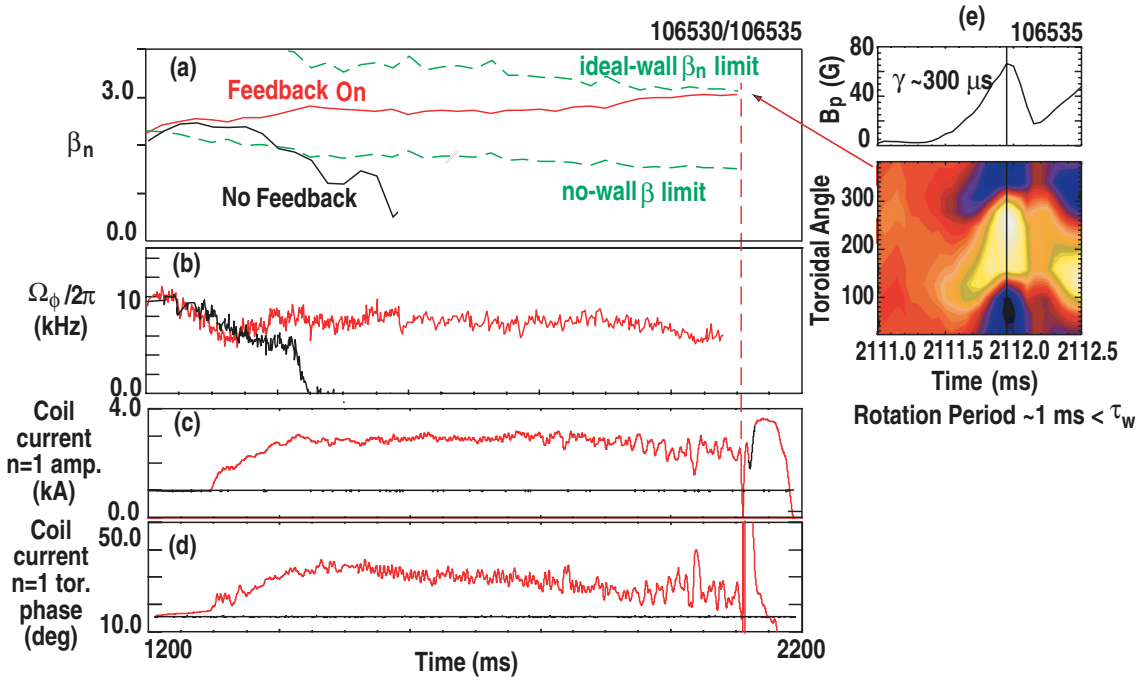

Fig. 11. Experimental achievement of high pressure plasma close to the ideal MHD limit. Shown in (a) are the traces of the plasma pressure (β_n) versus time in two discharges with/without feedback. The estimated ideal-wall and no-wall limits were verified by the GATO code using experimentally measured pressure and safety factor q- profiles. (b) The evolution in time of the rotation frequency for the two discharges with and without feedback. (c) The amplitude of the n=1 radial magnetic field supplied by the C-coil system. Note that with no feedback, the current is preset to be 2 kA. (d) The toroidal phase the n=1 radial magnetic field supplied by C-coil. Without feedback the toroidal angle is preset to 16°. (e) Growth of the n=1 poloidal field perturbation near the ideal MHD limit. The growth rate of the mode is observed to be 300 μs within this duration its toroidal phase angle also undergoes a 180° phase shift.

With the feedback off, yet when the C-coil currents were pre-programmed to those determined by the feedback system with feedback on, the discharge behavior as shown in Fig. 12 followed the evolution of the discharge with feedback on (Fig. 11). The achieved values of β_n and plasma rotation frequency were identical to the one with feedback on. This evidence suggests that the resonant component of residual non-axisymmetric field contributed significantly to the mode amplification and consequently reduced the rotation velocity. Once the compensation was made, the RFA did not grow and the plasma does not slow down. Plasma rotation was able to suppress the onset of RWM up to the ideal MHD β_n limit.

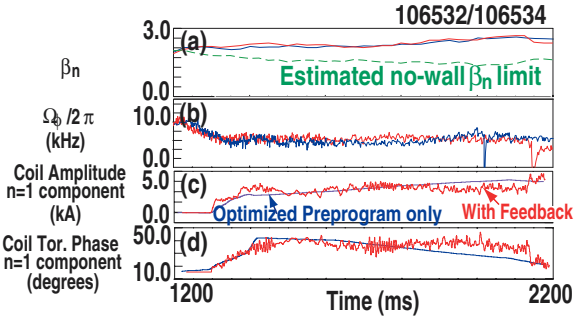

Fig. 12. Experimental achievement of high β_n discharge with preprogrammed coil current and the comparison to the case by using feedback. Two traces are shown, red is with and blue is without feedback. Shown in (a) is the plasma pressure (β_n) versus time. The dotted line shows the estimated no-wall β_n limit. Shown in (b) the plasma rotation, in (c) the amplitude of the n=1 component of the coil current, and in (d) the toroidal phase angle of the n=1 component of the coil current.

This approach is robust. It is further tested and a high β plasma was maintained with duration extended as shown in Fig. 13. In this case, the preprogrammed coil current was adjusted based on the feedback results discussed above. The plasma pressure and plasma current were slightly adjusted around 2.2 s to circumvent the ideal-wall β limit. The preprogrammed current was adequate for suppressing the onset of the RWM throughout the duration of the discharge. The discharge was sustained with $\beta_N \geq 50$ % above the no-wall β limit for more than 1.6 s, which is more than 10 times of plasma confinement time.

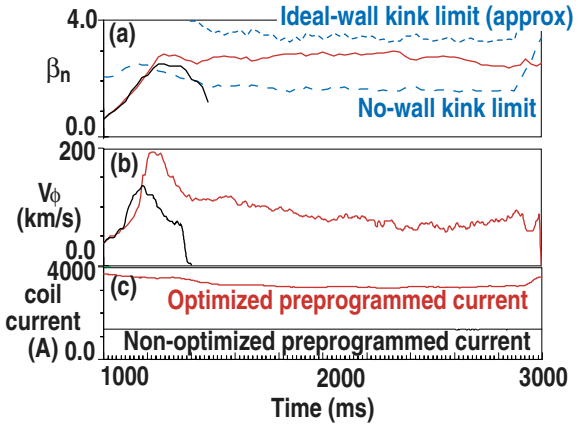

Fig. 13. Experimental demonstration of sustaining a high β_n discharge by using magnetic feedback (red curve). Note that this discharge lasted .8 sec longer than that shown in Fig. 12. For comparison, the trace of a similar discharge without using feedback is shown in blue. Shown in (a) is the plasma pressure (β_n) versus time. The dotted lines show the ideal-wall and no-wall kink limit. Shown in (b) is the plasma rotation at the q=2 surface versus time. Shown in (c) is the coil current in one(C79) of the -coils versus time.

V. FEEDBACK CONTROL OF THE FAST GROWING RWM

As shown in the previous sections, the resonant component of error field evolves slowly in time. To compensate the resonant component of the error field, a slow response from the feedback system seems adequate. In this section, we provide experimental evidence that the feedback system was also capable in suppressing the growth of a faster RWM, with an intrinsic growth rate which is faster than the rate of change of the external error field.

The performance of the feedback system on modes with a fast growth rate can be studied by using the feedback with a derivative gain. Figure 14 shows the results of feedback using the external δB_r saddle loops and with the smart shell logic [19]. Without feedback, at around 1400 ms, the RWM amplitude is observed to grow with a time constant = 4–5 ms, comparable to or slightly faster than the time constant given by the resistive wall. At saturation, the RWM amplitude reached 20 G. When feedback was activated with proportional (Gp) and derivative(Gd) feedback gains set to Gp = 5 and Gd = 11, the onset of RWM was delayed by 25 ms and then the amplitude reached a reduced level of 7–8 G. A further increase of the derivative gain to Gd = 14 and with the proportional gain remaining at Gp = 5, the onset of the RWM at around 1400 ms was eliminated and the residual level of the RWM was reduced to a saturated level of 1 G until a very fast RWM started its growth at 1510 ms. Since the proportional gain was kept constant, the achievement of a longer plasma duration by increase in Gd is most likely due to the stabilization or suppression of the fast growing RWM mode by the fast response of the feedback system. The final growth time was observed to be 1.3 ms. The observed growth time of 1–2 ms < (1/2-1/5) τ_w, does not differ much from that expected from the growth of an ideal MHD mode for an equilibrium slowly evolving in time.

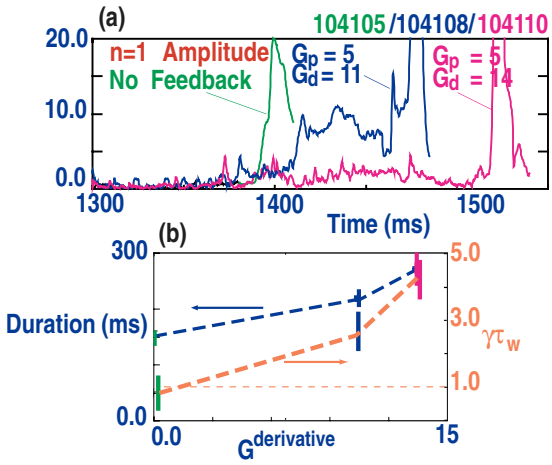

Fig. 14. Feedback stabilization of a fast growing RWM by using time derivative gain. The time constants for the proportional and the derivative gains were set at 0.4 ms. Shown in (a) are n=1 the amplitudes of the RWM versus time for three different shots: green for no feedback, blue for feedback with Gp (proportional gain) = 5, Gd (derivative gain) = 11, red for feedback with Gp = 5 and Gd = 14. It is seen that with a higher Gd, the discharge lasts longer, indicating that a RWM with a higher growth rate has been suppressed for a longer period by the higher derivative gain. Shown in (b) is the duration of the high β period (in blue) and the experimentally measured growth time (in orange) versus the value of the time derivative gain Gd. It is interesting to note that at Gd=14, the growth time of the RWM has been reduced to 1/3 of τ_w.

VI. SUMMARY

In this article, we reviewed first the basics of the RWM, the two methods for its stabilization, by using rotation and feedback. The phenomenon of RFA was introduced and the cylindrical lumped circuit model was extended as a basis for the quantitative description of RFA.

The RFA process was studied experimentally by the deliberate excitation of the C-coils to provide a known seed error field. The dissipation in the plasma has been found to be large and the plasma was in the strong dissipation regime wherein the kinetic energy is negligible. The experimental data can be described by the cylindrical lumped circuit model with a fixed dissipation coefficient α =2.5 μs and a critical β_0 value of β_0 = 1.5. However, the combination of α and β_0 was obtained under one particular plasma condition. It was also noticed that the critical β_0 determined from the RFA study was not close to the value of $\beta_n/\left(I/\pi a^2\right)$ =1 as predicted by Boozer in his original formulation. On the other hand, other unexpected plasma behavior such as strong beta collapse was observed near the $\left(I/\pi a^2\right)$ with critical rotation velocity. This may suggests that the critical β_n may depend on parameters such as plasma rotation other than just $\left(I/\pi a^2\right)$. In the DIII–D device, it was found feedback can be utilized to suppress RFA efficiently and reliably. The feedback system has been demonstrated to perform the multiple functions of finding the resonant residual non-axisymmetric field, compensating for the residue error fields, and to suppress the RFA and to maintain the plasma rotation. Maintaining sufficient plasma rotation stabilizes the plasma against the development of the RWM up to the ideal-wall β limit. Frequently, β_n reached values twice of that given by the no-wall limit, and was close to the ideal-wall MHD kink limit. This is, to the best of our knowledge, the first achievement of the ideal-wall pressure limit at such a high level of $\beta_n/\left(I/\pi a^2\right)$.

Once the residual component was found by the feedback system, the compensation needed for the reduction of the resonant component can be made with a pre-programmed C-coil currents. The approach for error field reduction is robust, as it uses the natural resonance of the MHD

mode near the marginal condition. This technique can be applied to other toroidal devices. One key element of the present success is the location of the actuator. On the DIII–D, the coil locations were originally chosen to compensate for the error field so that the elimination of the error field and the feedback stabilization of RFA/RWM can take place simultaneously by activating the feedback coils. It is very important to identify the error component and to locate the active coils in proper location for successful RWM control and RFA amelioration.

The principal stabilization mechanism demonstrated up to now for reaching high β seems to rely on rotational stabilization of the RWM. Here, we also reported experimental results using time derivative gain (Gd) to extend the plasma discharge duration. It suggests that the feedback system can also couple to the fast growing RWM. However, in future fusion devices, plasma rotation may not be sufficient for suppressing the growth rates of the RWM. Whether we can stabilize RWM up to the ideal wall limit under low rotation condition will be the next subject to be explore.

REFERENCES

[1] C. Kessel, et al., Phy. Rev. Lett. **72**,1212 (1994).

[2] S. Jardin, et. al., Fusion Eng. Des. **38**, 27 (1997).

[3] A. Turmbull, et al., Phyts. Rev. Lett. **74** 718 (1995).

[4] A. Bondeson and D. Ward, Phys. Rev. Lett. **72**, (1994) 2709.

[5] D. J. Ward and A. Bondeson, Phys. Plasmas **2**,1570(1995).

[6] R. Betti and J. P. Freiberg, Phy. Rev. Lett, **74**,2949 (1995).

[7] R. Fitzpatrick and A. Aydmir, Nucl. Fusion **36**, 11(1996).

[8] J. Finn ????

[9] C. Bishop, Plasma Physc. controlled Fusion **31**,2641 (1989).

[10] R. Fitzpatrick and T. Jensen, Phys. Plasmas **2**, 2641 (1996).

[11] C. Gimblett and R. J. Hastie, Phys. Plasmas **7**, 258 (2000).

[12] Y. O. Liu and A. Bondeson, Phy rev. Lett. **84**, 907 (2000).

[13] Y. O. Lie, et al., Phy. Plasmas **7**, 3681.

[14] R. Fizpatrick, "A Simple Model of the Resistive Wall Mode in Tokamaks," (private communication).

[15] E.J. Strait, et al., Phys. Rev. Lett. **74**, 2483 (1994).

[16] T. Taylor, et al., Phys. Plasmas **2**, 2390(1995).

[17] A.M. Garofalo, et al., Phys. Rev. Lett. **82**, 3811 (1999).

[18] A.M. Garofalo, et al., Nucl. Fusion **40**, 1491 (2000).

[19] M. Okabayashi, et al., Phys. Plasmas **8**, 2071 (2001).

[20] L. Johnson, et al., in "Structure and Feedback Stabilization of Resistive Wall Modes in DIII-D," in Proc. of the 28th EPS Conf. on Controlled Fusion and Plasma Physics, Madeira, 2001 (European Physical Society, Petit-Lancy, 2001).

[21] A.M. Garofalo, et al., Phy. Plasmas **9**, 1997(2001).

[22] A.M. Garofalo, R.J. La Haye, and J.T. Scoville, GA report. GA-A23849.

[23] A. Garofalo, et al.,GA report (2001) GA-A23849.

[24] A.M. Garofalo, et al., Nucl. Fusion **41**, 1171 (2001).

[25] A. Boozer, Phy. Rev. Lett. **86**, 1176 (2001).

[26] M.S. Chu, et al., Phys. Plasmas **2**, 2236 (1995).

[27] M. Okabayashi, N. Pomphrey and R. Hatcher, Nucl. Fusion **38**, 1607 (1998).

[28] M. Okabayashi, et al., "In the proceedings of The 12th International Toki conference on Plasma Physics and Controlled Nuclear Fusion" (Toki, Japan 2001, to be published).

[29] J. Bialek, et al., Phys. Plasmas **8**, 2170 (2001).

[30] A. Boozer, Phys. Plasmas **6**, 3180 (1999).

[31] G. L. Johns, M. S. Chance, et al., Nuclear Fusion **28** 881 (1988).

[32] J.D. Callen, et al., Phy. Plasmas **6**,2963 (1999).

ACKNOWLEDGMENT

Work supported by U.S. Department of Energy under Contracts DE-AC02-76CH03073, DE-AC03-99ER54463, and Grant DE-FG02-89ER53297. We are greatly thankful to the physicists, engineering staffs, technical staffs involved in this project. In particular, we would like to express our appreciation to the DIII–D operation group.